3D Tensorial Elastodynamics for Isotropic Media on Vertically Deformed Meshes: 1. Theory

Jeffrey Shragge[1,2]
[1] *Center for Wave Phenomena, Colorado School of Mines*
[2] *Formerly University of Western Australia*

ABSTRACT
Solutions of the equations of 3D isotropic elastodynamics in Cartesian coordinates form the key computational kernel for many applications of isotropic elastic reverse-time migration and full waveform inversion. However, there are numerous situations where solutions are required for computational domains characterized by non-Cartesian geometry, including when handling free-surface topography and irregular internal mesh boundaries such as a depth-varying water bottom. One solution strategy is to compute the elastodynamic response on vertically deformed meshes designed to incorporate irregular topology. By following a tensorial formulation, I develop a system of (semi-)analytic equations governing 3D elastodynamics in a stress-velocity formulation for a broad family of vertically deformed meshes automatically defined by Bézier interpolation functions between two or more non-intersecting surfaces. The analytic coordinate definition also leads to a corresponding analytic free-surface boundary condition as well as expressions for wavefield injection and extraction. Theoretical examples illustrate the utility of the tensorial approach in generating analytic equations of 3D elastodynamics and exact tensorial free-surface boundary conditions for scenarios involving free-surface topography and irregular internal boundaries. Numerical validation of the theoretical results are presented in a companion paper.

1 INTRODUCTION

Numerical solutions of isotropic elastodynamics are increasingly being used for a wide variety of 3D earth imaging and inversion problems within the exploration, microseismic, and earthquake seismology communities. One of the main drivers is a need to accurately model and reproduce the full-wavefield elastic phenomena that are the key computational kernels for such applications as elastic reverse-time migration (E-RTM) and full waveform inversion (E-FWI). Elastodynamics solutions are also being used to develop high-quality synthetic 3D elastic datasets (i.e., with more realistic amplitude versus angle response) that are important in the context of developing and validating new algorithms, examples of which include the SEG Advanced Modeling (SEAM) Phase II project.

While the majority of 3D elastic modeling efforts are undertaken on Cartesian solution domains, there are numerous situations where the computation of 3D elastodynamics responses on more generalized non-Cartesian meshes is desirable. Of particular interest to those working on 3D Earth imaging and inversion problems are solutions computed on vertically deformed meshes that straightforwardly adapt to most of the irregular topologies encountered in real-world applications. Such scenarios include handling free-surface topography or irregular internal boundaries (e.g., water bottom, salt bodies) that commonly arise in land and marine seismology applications, respectively.

There are a number of different classes of numerical methods able to generate solutions of 3D isotropic elastodynamics for scenarios typified by non-Cartesian geometry. These include finite-difference (Carcione, 1994; Komatitsch et al., 1996; Hestholm, 1999; Hestholm and Ruud, 2002; Hestholm et al., 2006; Zhang and Chen, 2006; Lombard et al., 2008; Appelö and Petersson, 2009; de la Puente et al., 2014), spectral-element (Faccioli et al., 1997; Komatitsch and Vilotte, 1998; Tromp et al., 2008), pseudo-spectral (Feng et al., 2007) and discontinuous Galerkin (Käser and Dumbser, 2006) approaches. Examples of the latter classes generally are characterized by their ability to simulate highly accurate wavefield solutions even for significantly deformed computational domains; however, these classes require computing often very complex 3D meshing solutions prior to seismic modeling, and have 3D simulation runs typified by high computational complexity. Both of these factors are significant when considering "production-

mode" scenarios involving (iterative) computation of thousands of 3D modeling runs (or more) to complete an overall E-RTM (or E-FWI) task.

On the other hand, finite-difference (FD) methods are fairly straightforward to implement on simple, rotated or fully staggered grids (FSGs), and have compact stencils for derivative operators for fairly high numerical orders of accuracy [e.g., nine points for a $O(\Delta x^8)$ solution]. Thus, they are well suited for use in highly parallelized and efficient accelerator-based numerical solutions. One of the main challenges associated with computing FD solutions on irregular grids, though, is implementing FD schemes that are both stable and numerically accurate for computational meshes characterized by moderate-to-strong roughness (i.e., short wavelength variations in mesh geometry) and skewness (degree of mesh non-orthogonality). These FD stability and accuracy issues become increasingly acute in the boundary regions of computational domains where applying conventional higher-order stencils is problematic.

Over the past decade, the development of stable and high-order FD approaches able to address these challenges [e.g., mimetic finite difference (MFD) operators (Castillo and Miranda, 2013; de la Puente et al., 2014; Shragge and Tapley, 2017, and references therein) applied on FSGs (Lebedev, 1964; Lisitsa and Vishnevskiy, 2010)] arguably has lead to renewed interest in applying FD operators for generating elastodynamics solutions for scenarios involving vertically deformed meshes. To generate these solutions practitioners generally follow one of two mathematical strategies: the tensorial or the chain-rule approach. Tensorial approaches pose elastodynamics problems and their subsequent numerical solutions directly on a generalized coordinate mesh. Though this can only require the same number of wavefield derivatives as Cartesian solutions (Komatitsch et al., 1996), additional memory variables generally are required to account for the non-Cartesian metric tensor (g^{ij}) and corresponding affine connection variables (i.e., Christoffel symbols of the second kind, Γ^i_{jk}). On the other hand, chain-rule approaches first compute the spatial derivatives in the generalized coordinate system before using the chain-rule to transform the result back onto the Cartesian mesh. These operations have an associated additional computational and memory overhead relative to solutions computed in Cartesian domains. Relative to the tensorial approach, 3D chain-rule applications have higher computational complexity, but generally lower memory requirements (Komatitsch et al., 1996). Thus, during an era of memory-bound computing, the chain-rule approach for simulating solutions of isotropic elastodynamics on vertically deformed meshes tended to be more widely applied.

The work presented herein re-examines the tensorial formulation of the 3D isotropic elastodynamics (Komatitsch et al., 1996) using a new mathematical strategy. Instead of specifying a numerical 3D mesh and then directly computing the corresponding geometric memory variables, I develop analytic expressions for the equations governing 3D isotropic elastodynamics for *all* admissible (i.e., C_2 differentiable) vertically deformed coordinate systems. Importantly, developing analytic expressions significantly reduces (or effectively eliminates) the memory requirements associated with the geometric variables in the tensorial approach (though at the cost of additional derivative calculations). A significant additional benefit of the analytic formulation is that it leads to a set of exact analytic expressions for the free-surface boundary condition (FSBC) for *all* admissible vertically deformed grids. The derived analytic FSBC is straightforward to implement for all meshes characterized by a linear vertical deformation, and is applicable more generally when using a MFD+FSG strategy.

The paper begins with the tensorial theory of elastodynamics (for which a mathematical primer is provided in Appendix A), which is followed by the development of analytic equations of elastodynamics on the generalized family of vertically deformed coordinate systems. Then, I develop the analytic equations for the stress-velocity formulation for three example coordinate systems: two associated with free-surface topography, and a third related to internal mesh boundaries. The paper concludes with a discussion on some items to consider when following the prescribed tensorial elastodynamics approach. Validation of the advocated MFD+FSB numerical approach through comparison with analytical solutions, as well as presentation of numerical examples, are provided in a companion paper.

2 TENSORIAL FORMULATION OF 3D ELASTODYNAMICS

Numerical solutions of 3D elastodynamics are commonly computed using a stress-velocity numerical strategy. Herein, I follow a tensorial stress-velocity formulation that specifies the two governing equations that couple the stress tensor and particle velocity variables: the conservation of linear momentum and the stress-strain constitutive relationship. The theory presented in this section largely follows that of Komatitsch et al. (1996), which details the development and subsequent solution of a 2D tensorial stress-velocity elastodynamics formulation (though the described approach is generalizable to 3D implementations). The tensorial approach formulates the equations of elastodynamics in a generalized 3D coordinate system ($\boldsymbol{\xi}$) that is related to an underlying Cartesian mesh ($\boldsymbol{x}$) through invertible forward and inverse coordinate transforms, $x^i = x^i(\boldsymbol{\xi})$ and $\xi^i = \xi^i(\boldsymbol{x})$. Readers unfamiliar with the tensorial mathematics used in the development below are referred to the overview presented in Appendix A.

2.1 Conservation of Linear Momentum

The tensorial formulation of the conservation of linear momentum is given by (McConnell, 1957; Brillouin, 1964):

$$\rho \dot{v}_i = \nabla_j \sigma_i^j + f_i, \tag{1}$$

where $\rho = \rho(\boldsymbol{\xi})$ is density; $\dot{v}_i = \dot{v}_i(\boldsymbol{\xi})$ is particle acceleration (i.e., temporal derivative of particle velocity) in the ith direction; ∇_j is the covariant derivative defined in $\boldsymbol{\xi}$-coordinates; $f_i = f_i(\boldsymbol{\xi})$ is a covariant component of the force source vector; and $\sigma_i^j = \sigma_i^j(\boldsymbol{\xi})$ is the mixed (1,1) stress tensor. Temporal derivatives are represented by variables with an overlying dot. Summation notation is assumed over repeated upper and lower indices. Inserting the expression for the covariant derivative of the mixed tensor field (equation A.9) into the 3D elastodynamics equations yields

$$\rho \dot{v}_i = \frac{\partial \sigma_i^j}{\partial \xi^j} + \Gamma_{jk}^j \sigma_i^k - \Gamma_{ji}^k \sigma_k^j + f_i. \tag{2}$$

The Christoffel symbols, Γ_{jk}^i, are required to account for the spatial variation in how the underlying coordinate system expands, contracts or undergoes local shear deformation. Thus, these terms are identically zero in applications involving a spatially invariant Cartesian mesh.

2.2 Stress-strain constitutive relationship

The constitutive relationship between the stress-strain relationship for a 3D isotropic elastic medium in a mixed tensor (1,1) format is

$$\dot{\sigma}_i^j = \lambda\, \delta_i^j \dot{\epsilon}_k^k + 2\mu \dot{\epsilon}_i^j, \tag{3}$$

where λ and μ are Lamé parameters, and ϵ_i^j is the mixed (1,1) infinitesimal strain tensor. The strain tensor can be expressed in a covariant basis by lowering the raised index through multiplication of the contravariant metric tensor (equation A-4)

$$\dot{\epsilon}_i^j = g^{nj} \dot{\epsilon}_{in}, \tag{4}$$

which results in the following expression for isotropic stress tensor:

$$\dot{\sigma}_i^j = \lambda \delta_i^j g^{kn} \dot{\epsilon}_{nk} + 2\mu g^{kj} \dot{\epsilon}_{ik}. \tag{5}$$

The covariant representation of the infinitesimal strain tensor can be written

$$\dot{\epsilon}_{ik} = \frac{1}{2}\left(\nabla_i v_k + \nabla_k v_i\right) = \frac{1}{2}\left(\frac{\partial v_k}{\partial \xi^i} + \frac{\partial v_i}{\partial \xi^k}\right) - \Gamma_{ik}^l v_l, \tag{6}$$

where the symmetry of the Christoffel symbol (i.e., $\Gamma_{jk}^i = \Gamma_{kj}^i$) is used to consolidate multiple components into a single contribution. Combining the above expressions yields the following expression for the temporal derivative of the stress tensor in generalized 3D coordinates:

$$\begin{aligned} \dot{\sigma}_i^j \;=\; & \lambda \delta_i^j g^{kn} \left[\frac{1}{2}\left(\frac{\partial v_k}{\partial \xi^n} + \frac{\partial v_n}{\partial \xi^k}\right) - \Gamma_{nk}^l v_l\right] + \\ & 2\mu g^{kj} \left[\frac{1}{2}\left(\frac{\partial v_k}{\partial \xi^i} + \frac{\partial v_i}{\partial \xi^k}\right) - \Gamma_{ik}^l v_l\right]. \end{aligned} \tag{7}$$

2.3 Challenges for staggered-grid implementations

Equations 2 and 7 represent the two key relationships used for simulating numerical solutions of the 3D elastodynamic wave-equation in a stress-velocity formulation. In either equation, the right-hand side (RHS) contains spatial derivatives of the stress or velocity variables, while the expressions on the left-hand side (LHS) represent the temporal derivatives of these variables. However, note that the RHS of equation 2 contains components that are functions of both stress and its spatial derivatives, σ_i^j and $\frac{\partial \sigma_i^j}{\partial \xi^j}$. Likewise, the RHS of 7 contains components that are both functions of particle velocity and its spatial derivatives, v_i and $\frac{\partial v_i}{\partial \xi^k}$. These observations run counter to the design goals of staggered grid implementations because the respective sets of variables would fall on incompatible grid staggerings. Thus, in order to obtain a memory-efficient stress-velocity implementation one needs to explicitly define a 3D $\boldsymbol{\xi}$-coordinate system that leads to specific expressions for Christoffel symbols that have: (1) no RHS dependence on either σ_j^i or v_i; and (2) are solely functions of the stress and particle velocity derivatives.

3 3D ELASTODYNAMICS OF VERTICALLY DEFORMED COORDINATES

This section develops analytic expressions for elastodynamics that satisfies the above two criteria. To achieve this, I define a family of 3D coordinate systems with a stretch associated with one axis, herein assumed to be vertical. No additional stretching is applied in the other two coordinate axes. These types of coordinates can be used to represent a variety of different scenarios including free-surface topography and various internal boundary geometries.

I begin by specifying and examining the "geometric attributes" of the general family of vertically deformed 3D $\boldsymbol{\xi}$-coordinate systems. I then develop analytic expressions for temporal derivative of the 3D stress tensor and conservation of linear momentum equations. After deriving an exact expression for the free-surface boundary condition for these generalized coordinate transformations, this section concludes with the relationships required for injecting or extracting vector wavefield energy.

3.1 3D Vertically Deformed Meshes

A family of 3D vertically stretched coordinate systems can defined by the following transformation [also known as a Monge parameterization (Guo, 2014)]

$$\mathbf{x} = \begin{bmatrix} x^1 \\ x^2 \\ x^3 \end{bmatrix} = \begin{bmatrix} F\left(\xi^1,\xi^2,\xi^3\right) \\ \xi^2 \\ \xi^3 \end{bmatrix}, \tag{8}$$

where $F = F\left(\xi^1,\xi^2,\xi^3\right)$ is a yet to be specified generalized function of the three coordinate variables representing the vertical deformation. (Note that the scenario where $F = \xi^1$ represents a Cartesian coordinate system.) To develop an analytic set of governing elastodynamics equations for this family of generalized coordinates, one must first define expressions for the inverse metric tensor, g^{ij}, and Christoffel symbols of the second kind, Γ^i_{jk}. Using a notation where $F_i \equiv \frac{\partial F}{\partial \xi^i}$ and $F_{i,j} \equiv \frac{\partial^2 F}{\partial \xi^i \partial \xi^j}$, the inverse metric tensor may be written

$$\left[g^{ij}\right] = \frac{1}{F_1}\begin{bmatrix} F_1^{-1}\left(1+F_2^2+F_3^2\right) & -F_2 & -F_3 \\ -F_2 & 1 & 0 \\ -F_3 & 0 & 1 \end{bmatrix}, \tag{9}$$

while the associated Christoffel symbols are given by

$$\begin{bmatrix} \Gamma^1_{jk} \\ \Gamma^2_{jk} \\ \Gamma^3_{jk} \end{bmatrix} = \frac{1}{F_1}\begin{bmatrix} F_{j,k} \\ 0 \\ 0 \end{bmatrix}. \tag{10}$$

I note that the straightforward coordinate transformation in equation 8 generates a fairly sparse set of geometric objects that are dependent solely on the spatial first- and second-order partial derivatives of the particular choice of coordinate stretch function, F. Substituting these results allows the equation of 3D conservation of linear momentum and isotropic stress-strain relationship to be rewritten as

$$\rho\dot{v}_i = \frac{\partial \sigma_i^j}{\partial \xi_j} + \frac{1}{F_1}\left[F_{1,k}\sigma_i^k - F_{i,j}\sigma_1^j\right] + f_i, \tag{11}$$

$$\dot{\sigma}_i^j = \lambda\delta_i^j g^{kn}\left[\frac{1}{2}\left(\frac{\partial v_k}{\partial \xi^n} + \frac{\partial v_n}{\partial \xi^k}\right) - \frac{F_{n,k}}{F_1}v_1\right] + 2\mu g^{kj}\left[\frac{1}{2}\left(\frac{\partial v_k}{\partial \xi^i} + \frac{\partial v_i}{\partial \xi^k}\right) - \frac{F_{i,k}}{F_1}v_1\right], \tag{12}$$

where the subscript 1 is introduced through the upper index of the non-zero Christoffel symbols in equation 10. To remove the explicit dependence on fields v_i and σ_i^j, I use the chain rule to shift the partial derivatives, e.g.:

$$\sigma_k^j\left(F_i\right)_{,j} = \left(F_i\sigma_k^j\right)_{,j} - F_i\left(\sigma_k^j\right)_{,j}. \tag{13}$$

This allows the equations governing 3D isotropic elastodynamics to be written

$$\rho\dot{v}_i = \frac{\partial \sigma_i^j}{\partial \xi_j} + f_i + \frac{1}{F_1}\left[\frac{\partial(F_1\sigma_i^k)}{\partial \xi^k} - F_1\frac{\partial \sigma_i^k}{\partial \xi^k} - \frac{\partial(F_i\sigma_1^j)}{\partial \xi^j} + F_i\frac{\partial \sigma_1^j}{\partial \xi^j}\right], \tag{14}$$

$$\dot{\sigma}_i^j = \frac{\lambda\delta_i^j g^{kn}}{2}\left[\frac{\partial v_k}{\partial \xi^n} + \frac{\partial v_n}{\partial \xi^k} - \frac{2}{F_1}\frac{\partial(F_n v_1)}{\partial \xi^k} + \frac{2F_n}{F_1}\frac{\partial v_1}{\partial \xi^k}\right] + \mu g^{kj}\left[\frac{\partial v_k}{\partial \xi^i} + \frac{\partial v_i}{\partial \xi^k} - \frac{2}{F_1}\frac{\partial(F_i v_1)}{\partial \xi^k} + \frac{2F_i}{F_1}\frac{\partial v_1}{\partial \xi^k}\right], \tag{15}$$

which forms a system of equations where the RHS is now explicitly dependent on the spatial partial derivatives of stresses and particle velocities and not on the quantities themselves. Accordingly, this formulation of 3D elastodynamics is now consistent with the requirement of formulating memory efficient (and symmetric) stress-velocity staggered grid solution - though at the cost of an increased number of required partial derivative evaluations.

3.2 Stress Tensor Components

While the temporal derivative of the stress tensor is written in a compact form in equation 15, it is advantageous to evaluate and simplify the expression for each of the nine tensor components. This requires computing the intermediate results of: (1) inserting the metric tensor into the covariant strain tensor in equation 6; and (2) applying the raising the index of the result of (1) to a mixed strain tensor representation. The final step is to introduce the result of (2) into the isotropic elastic constitutive relationship given in equation 7 to yield the following expressions of the temporal derivative of the mixed stress tensor $\dot{\sigma}_j^i$:

$$\frac{\dot{\sigma}_1^1}{\lambda} = \frac{E_{1,1}}{F_1}\frac{\partial\left(F_1\gamma_F v_1\right)}{\partial \xi^1} + E_{0,1}\gamma_F\left[2\frac{\partial v_1}{\partial \xi^1} - \frac{1}{F_1}\frac{\partial\left(F_1 v_1\right)}{\partial \xi^1}\right] + \frac{\partial v_2}{\partial \xi^2} + \frac{\partial v_3}{\partial \xi^3} - \frac{E_{0,1}}{F_1}\left[F_2\frac{\partial v_1}{\partial \xi^2} + F_3\frac{\partial v_1}{\partial \xi^3}\right] - \frac{E_{1,1}}{F_1}\left[F_2\frac{\partial v_2}{\partial \xi^1} + F_3\frac{\partial v_3}{\partial \xi^1}\right] - \frac{1}{F_1}\left[\frac{\partial\left(F_2 v_1\right)}{\partial \xi^2} + \frac{\partial\left(F_3 v_1\right)}{\partial \xi^3}\right] \tag{16}$$

$$\frac{\dot{\sigma}_2^1}{\mu} = \gamma_F\frac{\partial v_2}{\partial \xi^1} - \frac{2F_2}{F_1}\frac{\partial v_2}{\partial \xi^2} - \frac{F_3}{F_1}\left[\frac{\partial v_2}{\partial \xi^3} + \frac{\partial v_3}{\partial \xi^2}\right] + \frac{\partial\left(\gamma_F v_1\right)}{\partial \xi^2} \tag{17}$$

$$\frac{\dot{\sigma}_3^1}{\mu} = \gamma_F\frac{\partial v_3}{\partial \xi^1} - \frac{2F_3}{F_1}\frac{\partial v_3}{\partial \xi^3} - \frac{F_2}{F_1}\left[\frac{\partial v_2}{\partial \xi^3} + \frac{\partial v_3}{\partial \xi^2}\right] + \frac{\partial\left(\gamma_F v_1\right)}{\partial \xi^3} \tag{18}$$

$$\frac{\dot{\sigma}_1^2}{\mu} = \frac{\partial v_1}{\partial \xi^2} + \frac{\partial v_2}{\partial \xi^1} - 2\frac{\partial\left(F_1^{-1}F_2 v_1\right)}{\partial \xi^1} \tag{19}$$

$$\frac{\dot{\sigma}_2^2}{\lambda} = \frac{1}{F_1}\frac{\partial\left(F_1\gamma_F v_1\right)}{\partial\xi^1} + E_{1,2}\frac{\partial v_2}{\partial\xi^2} + \frac{\partial v_3}{\partial\xi^3} - \frac{F_3}{F_1}\frac{\partial v_3}{\partial\xi^1} + \frac{F_2}{F_1}\left[E_{0,1}\frac{\partial v_1}{\partial\xi^2} - E_{1,1}\frac{\partial v_2}{\partial\xi^1}\right] - \frac{1}{F_1}\left[\frac{\partial(F_3 v_1)}{\partial\xi^3} + E_{1,2}\frac{\partial(F_2 v_1)}{\partial\xi^2}\right] + \frac{E_{0,1}}{F_1^2}\left[\frac{\partial\left(F_2^2 v_1\right)}{\partial\xi^1} - F_2^2\frac{\partial v_1}{\partial\xi^1}\right] \quad (20)$$

$$\frac{\dot{\sigma}_3^2}{\mu} = \frac{\partial v_2}{\partial\xi^3} + \frac{\partial v_3}{\partial\xi^2} + \frac{F_2}{F_1}\left[\frac{\partial v_1}{\partial\xi^3} - \frac{\partial v_3}{\partial\xi^1}\right] - 2\frac{\partial\left(F_1^{-1}F_2 v_1\right)}{\partial\xi^3} \quad (21)$$

$$\frac{\dot{\sigma}_1^3}{\mu} = \frac{\partial v_1}{\partial\xi^3} + \frac{\partial v_3}{\partial\xi^1} - 2\frac{\partial\left(F_1^{-1}F_3 v_1\right)}{\partial\xi^1} \quad (22)$$

$$\frac{\dot{\sigma}_2^3}{\mu} = \frac{\partial v_2}{\partial\xi^3} + \frac{\partial v_3}{\partial\xi^2} + \frac{F_3}{F_1}\left[\frac{\partial v_1}{\partial\xi^2} - \frac{\partial v_2}{\partial\xi^1}\right] - 2\frac{\partial\left(F_1^{-1}F_3 v_1\right)}{\partial\xi^2} \quad (23)$$

$$\frac{\dot{\sigma}_3^3}{\lambda} = \frac{1}{F_1}\frac{\partial\left(F_1\gamma_F v_1\right)}{\partial\xi^1} + \frac{\partial v_2}{\partial\xi^2} + E_{1,2}\frac{\partial v_3}{\partial\xi^3} - \frac{F_2}{F_1}\frac{\partial v_2}{\partial\xi^1} + \frac{F_3}{F_1}\left[E_{0,1}\frac{\partial v_1}{\partial\xi^3} - E_{1,1}\frac{\partial v_3}{\partial\xi^1}\right] - \frac{1}{F_1}\left[\frac{\partial(F_2 v_1)}{\partial\xi^2} + E_{1,2}\frac{\partial(F_3 v_1)}{\partial\xi^3}\right] + \frac{E_{0,1}}{F_1^2}\left[\frac{\partial\left(F_3^2 v_1\right)}{\partial\xi^1} - F_3^2\frac{\partial v_1}{\partial\xi^1}\right], \quad (24)$$

where $\gamma_F = F_1^{-2}\left(1 + F_2^2 + F_3^2\right)$ and $E_{a,b} = \frac{a\lambda + b\mu}{\lambda}$ are used for notational compactness. The stress tensor components expressed in equations 17-24 are valid for any admissible choice of vertical deformation function F.

3.3 Conservation of Linear Momentum

It is similarly advantageous to evaluate the geometric expressions and simplify the three equations of conservations of linear momentum given in equation 14. There is one intermediate step of evaluating the covariant derivative of mixed stress tensor, $\sigma^i_{j,k}$. The simplified equations of 3D conservation of linear momentum are given by the following three expressions:

$$\rho\dot{v}_1 = \frac{\partial\sigma_1^1}{\partial\xi_1} + \frac{\partial\sigma_1^2}{\partial\xi_2} + \frac{\partial\sigma_1^3}{\partial\xi_3} + f_1 \quad (25)$$

$$\rho\dot{v}_2 = 2\frac{\partial\sigma_2^2}{\partial\xi_2} - \frac{\partial\sigma_1^1}{\partial\xi_2} + \frac{1}{F_1}\left[\frac{\partial(F_1\sigma_2^1)}{\partial\xi_1} + \frac{\partial(F_1\sigma_2^3)}{\partial\xi_3}\right] + F_1\frac{\partial\left(F_1^{-1}(\sigma_1^1 - \sigma_2^2)\right)}{\partial\xi_2} + \frac{F_2}{F_1}\frac{\partial\sigma_1^2}{\partial\xi_2} + \frac{F_3}{F_1}\frac{\partial\sigma_1^3}{\partial\xi_2} - \frac{1}{F_1}\frac{\partial\left(F_2\sigma_1^2 + F_3\sigma_1^3\right)}{\partial\xi_2} + f_2 \quad (26)$$

$$\rho\dot{v}_3 = 2\frac{\partial\sigma_3^3}{\partial\xi_3} - \frac{\partial\sigma_1^1}{\partial\xi_3} + \frac{1}{F_1}\left[\frac{\partial(F_1\sigma_3^1)}{\partial\xi_1} + \frac{\partial(F_1\sigma_3^2)}{\partial\xi_2}\right] + F_1\frac{\partial(F_1^{-1}(\sigma_1^1 - \sigma_3^3))}{\partial\xi_3} + \frac{F_2}{F_1}\frac{\partial\sigma_1^2}{\partial\xi_3} + \frac{F_3}{F_1}\frac{\partial\sigma_1^3}{\partial\xi_3} - \frac{1}{F_1}\frac{\partial(F_2\sigma_1^2 + F_3\sigma_1^3)}{\partial\xi_3} + f_3. \quad (27)$$

Again, these expressions are valid for any admissible choice of vertical deformation function F.

3.4 Free-surface Boundary Condition

One of the challenges of using FD approaches for generating wavefield solutions of non-Cartesian 3D elastodynamics is enforcing correct elastic wavefield behavior at the free surface through the so-called free-surface boundary condition (FSBC). The tensorial expression for the 3D FSBC is given by:

$$\sigma_i^j n_j\,\big|_{\xi^1=0} = 0, \quad i = 1,2,3, \quad (28)$$

where n_j is assumed to be normal to the free surface at $\xi_1 = 0$. Note that for a vertically deformed mesh the orientation of the free-surface normal is not generally aligned with grid. Thus, one must account for the non-orthogonality of the coordinate mesh also at the free surface. The unit normal $\mathbf{n}$ to the free surface is given by

$$\mathbf{n} = \frac{e_2\times e_3}{|e_2\times e_3|} = \frac{e_2\times e_3}{\sqrt{|g|}} = \frac{1}{\sqrt{1+F_2^2+F_3^2}}\begin{bmatrix}1\\-F_2\\-F_3\end{bmatrix}, \quad (29)$$

where

$$e_2 = \frac{\partial\mathbf{x}}{\partial\xi_2} = \begin{bmatrix}F_2\\1\\0\end{bmatrix}, \quad e_3 = \frac{\partial\mathbf{x}}{\partial\xi_3} = \begin{bmatrix}F_3\\0\\1\end{bmatrix}, \quad (30)$$

where these quantities are evaluated at $\xi_1 = 0$. Substituting the above mixed stress tensor components into equation 28 yields a system of three equations that can be solved exactly for the three unspecified derivatives of particle velocity in the ξ_1 direction (i.e., $\frac{\partial v_i}{\partial\xi_1}$). The general solution for the family of vertically deformed meshes given by equation 8 may be computed via:

$$\frac{\partial v_1}{\partial\xi^1} = v_1\frac{F_{1,1}}{F_1} + F_1\zeta_F \quad (31)$$

$$\quad (32)$$

$$\frac{\partial v_2}{\partial\xi^1} = -3\frac{\partial v_1}{\partial\xi^2} + \frac{2}{F_1}\frac{\partial(F_1 v_1)}{\partial\xi_2} + 2F_2\zeta_F \quad (33)$$

$$\quad (34)$$

$$\frac{\partial v_3}{\partial\xi^1} = -3\frac{\partial v_1}{\partial\xi^3} + \frac{2}{F_1}\frac{\partial(F_1 v_1)}{\partial\xi_3} + 2F_3\zeta_F \quad (35)$$

where

$$\zeta_F = -E^{-1}_{(1-F_2^2-F_3^2),2}\left[F_2\frac{\partial v_1}{\partial \xi^2} + F_3\frac{\partial v_1}{\partial \xi^3} + ... \right. \quad (36)$$
$$\left. F_1\left(\frac{\partial v_2}{\partial \xi^2} + \frac{\partial v_3}{\partial \xi^3}\right) - \frac{\partial (F_2 v_1)}{\partial \xi_2} - \frac{\partial (F_3 v_1)}{\partial \xi_3}\right].$$

All quantities in equations 31-36 are again evaluated at the free surface (i.e., $\xi^1 = 0$). Note that the first term on the RHS in equation 31a cannot be eliminated using a chain-rule substitution of an appropriate partial differential expression. However, the dependence on this term will be removed for any coordinate system involving constant or linear mappings in the ξ^1 direction (i.e., where $F_{1,1} = 0$). For completeness, substituting the expressions for Cartesian coordinates (i.e., $F = \xi^1$, $F_i = \delta^i_1$) recovers

$$\frac{\partial v_1}{\partial \xi^1} = -E^{-1}_{1,2}\left(\frac{\partial v_2}{\partial \xi^2} + \frac{\partial v_3}{\partial \xi^3}\right) \quad (37)$$

$$\frac{\partial v_2}{\partial \xi^1} = -\frac{\partial v_1}{\partial \xi^2} \quad (38)$$

$$\frac{\partial v_3}{\partial \xi^1} = -\frac{\partial v_1}{\partial \xi^3}, \quad (39)$$

which are the familiar FSBCs for 3D Cartesian implementations of isotropic elastodynamics.

3.5 Injection/Extraction of Wavefield Energy

Injecting a force source, f_i, specified in Cartesian coordinates requires first transforming this vector field to the vertically stretched domain. Using the expression detailed in equation A.5 yields the following $\boldsymbol{\xi}$-coordinate expression:

$$\left[\begin{array}{c} v_1 \\ v_2 \\ v_3 \end{array}\right]\Bigg|_{\boldsymbol{\xi}_0} = \left[\begin{array}{c} F_1 v_1 \\ v_2 + F_2 v_1 \\ v_3 + F_3 v_1 \end{array}\right]\Bigg|_{\boldsymbol{x}_0}, \quad (40)$$

where $\boldsymbol{x}_0$ and $\boldsymbol{\xi}_0$ are the equivalent points in the $\boldsymbol{x}$ and $\boldsymbol{\xi}$ coordinate systems. Similarly, extracting the particle velocity components from the computational grid requires evaluating the inverse transformation from vertically deformed coordinates back to Cartesian variables. The analytic inverse of equation 40 is

$$\left[\begin{array}{c} v_1 \\ v_2 \\ v_3 \end{array}\right]\Bigg|_{\boldsymbol{x}_0} = \frac{1}{F_1}\left[\begin{array}{c} v_1 \\ v_2 - F_2 v_1 \\ v_3 - F_3 v_1 \end{array}\right]\Bigg|_{\boldsymbol{\xi}_0}. \quad (41)$$

This generally non-orthogonal projection is computed prior to any interpolation of wavefield components to the physical $\boldsymbol{x}$ domain for visualization purposes.

4 ANALYTIC EXAMPLES

4.1 Example 1: Unstretched Topography

This section presents the example of 3D "unstretched" topographic coordinates, which is the most straightforward mapping that can accommodate irregular free-surface topography. An unstretched topographic coordinate mapping may be defined by

$$F\left(\xi^1, \xi^2, \xi^3\right) = \xi^1 + T(\xi^2, \xi^3), \quad (42)$$

where $T = T(\xi^2 = x^2, \xi^3 = x^3)$ is the map of the topography at the free surface (i.e., $\xi^1 = 0$). Figure 1 provides an example of a depth section through an unstretched topographic coordinates. Note that in this mapping each depth level in the mesh exhibits an imprint of the topographic surface, but is successively shifted to greater depth by increment $\Delta\xi_1$. The derivative expressions of the F field are $F_1 = 1$, $F_2 = T_2$ and $F_3 = T_3$. These expressions simplify the stress-rate equations 17-24 to

$$\frac{\dot{\sigma}^1_1}{\lambda} = E_{1,2}\gamma_T\frac{\partial v_1}{\partial \xi^1} + \frac{\partial\left(v_2 - T_2 v_1\right)}{\partial \xi^2} + \frac{\partial\left(v_3 - T_3 v_1\right)}{\partial \xi^3}$$
$$-E_{0,1}\left[T_2\frac{\partial v_1}{\partial \xi^2} + T_3\frac{\partial v_1}{\partial \xi^3}\right] \quad (43)$$
$$-E_{1,1}\left[T_2\frac{\partial v_2}{\partial \xi^1} + T_3\frac{\partial v_3}{\partial \xi^1}\right],$$

$$\frac{\dot{\sigma}^1_2}{\mu} = \frac{\partial(\gamma_T v_1)}{\partial \xi^2} + \gamma_T\frac{\partial v_2}{\partial \xi^1} - 2T_2\frac{\partial v_2}{\partial \xi^2} - T_3\left[\frac{\partial v_2}{\partial \xi^3} + \frac{\partial v_3}{\partial \xi^2}\right], \quad (44)$$

$$\frac{\dot{\sigma}^1_3}{\mu} = \frac{\partial(\gamma_T v_1)}{\partial \xi^3} + \gamma_T\frac{\partial v_3}{\partial \xi^1} - 2T_3\frac{\partial v_3}{\partial \xi^3} - T_2\left[\frac{\partial v_2}{\partial \xi^3} + \frac{\partial v_3}{\partial \xi^2}\right], \quad (45)$$

$$\frac{\dot{\sigma}^2_1}{\mu} = \frac{\partial v_1}{\partial \xi^2} + \frac{\partial v_2}{\partial \xi^1} - 2T_2\frac{\partial v_1}{\partial \xi^1}, \quad (46)$$

$$\frac{\dot{\sigma}^2_2}{\lambda} = \gamma_T\frac{\partial v_1}{\partial \xi^1} + E_{1,2}\frac{\partial(v_2 - T_2 v_1)}{\partial \xi^2} + \frac{\partial(v_3 - T_3 v_1)}{\partial \xi^3}$$
$$-T_3\frac{\partial v_3}{\partial \xi^1} + T_2\left[E_{0,1}\frac{\partial v_1}{\partial \xi^2} - E_{1,1}\frac{\partial v_2}{\partial \xi^1}\right], \quad (47)$$

$$\frac{\dot{\sigma}^2_3}{\mu} = \frac{\partial v_3}{\partial \xi^2} + \frac{\partial v_2}{\partial \xi^3} - 2\frac{\partial\left(T_2 v_1\right)}{\partial \xi^3} + T_2\left[\frac{\partial v_1}{\partial \xi^3} - \frac{\partial v_3}{\partial \xi^1}\right], \quad (48)$$

$$\frac{\dot{\sigma}^3_1}{\mu} = \frac{\partial v_1}{\partial \xi^3} + \frac{\partial v_3}{\partial \xi^1} - 2T_3\frac{\partial v_1}{\partial \xi^1}, \quad (49)$$

$$\frac{\dot{\sigma}^3_2}{\mu} = \frac{\partial v_2}{\partial \xi^3} + \frac{\partial v_3}{\partial \xi^2} - 2\frac{\partial\left(T_3 v_1\right)}{\partial \xi^2} + T_3\left[\frac{\partial v_1}{\partial \xi^2} - \frac{\partial v_2}{\partial \xi^1}\right], \quad (50)$$

$$\frac{\dot{\sigma}^3_3}{\lambda} = \gamma_T\frac{\partial v_1}{\partial \xi^1} + \frac{\partial(v_2 - T_2 v_1)}{\partial \xi^2} + E_{1,2}\frac{\partial(v_3 - T_3 v_1)}{\partial \xi^3}$$
$$-T_2\frac{\partial v_2}{\partial \xi^1} + T_3\left[E_{0,1}\frac{\partial v_1}{\partial \xi^3} - E_{1,1}\frac{\partial v_3}{\partial \xi^1}\right], \quad (51)$$

where $\gamma_T = 1 + T_2^2 + T_3^2$ and $E_{a,b} = \frac{a\lambda + b\mu}{\lambda}$ is used to abbreviate the Lamé parameter contributions.

Note that these equations involve 12 memory variables, two elastic fields (λ and μ), and require 15 different 3D derivative calculations [i.e., (1) nine $v_{i,j}$; (2) four T_j weighted derivatives: $(T_2 v_1)_{,2}$, $(T_2 v_1)_{,3}$, $(T_3 v_1)_{,2}$ and $(T_2 v_1)_{,3}$; and (3) two T_j^2 weighted derivatives: $((T_2^2 + T_3^2) v_1)_{,2}$ and $((T_2^2 + T_3^2) v_1)_{,3}$]. The only memory variables associated with irregular geometry are the 2D T_2 and T_3 fields. Otherwise, there is no functional dependence on coordinate system geometry.

Similarly, the conservation of linear momentum equations simplify to

$$\rho \dot{v_1} = \frac{\partial \sigma_1^1}{\partial \xi_1} + \frac{\partial \sigma_1^2}{\partial \xi_2} + \frac{\partial \sigma_1^3}{\partial \xi_3} + f_1, \tag{52}$$

$$\begin{aligned} \rho \dot{v_2} = & \frac{\partial \sigma_2^1}{\partial \xi_1} + \frac{\partial \sigma_2^2}{\partial \xi_2} + \frac{\partial \sigma_2^3}{\partial \xi_3} \\ & + T_2 \frac{\partial \sigma_1^2}{\partial \xi_2} + T_3 \frac{\partial \sigma_1^3}{\partial \xi_2} - \frac{\partial \left(T_2 \sigma_1^2 + T_3 \sigma_1^3 \right)}{\partial \xi_2} + f_2, \end{aligned} \tag{53}$$

$$\begin{aligned} \rho \dot{v_3} = & \frac{\partial \sigma_3^1}{\partial \xi_1} + \frac{\partial \sigma_3^2}{\partial \xi_2} + \frac{\partial \sigma_3^3}{\partial \xi_3} \\ & + T_2 \frac{\partial \sigma_1^2}{\partial \xi_3} + T_3 \frac{\partial \sigma_1^3}{\partial \xi_3} - \frac{\partial \left(T_2 \sigma_1^2 + T_3 \sigma_1^3 \right)}{\partial \xi_3} + f_3. \end{aligned} \tag{54}$$

The solution of these equations again involve all 12 memory variables (plus density field ρ), and a total of 13 partial derivative evaluations of the (weighted) stress field variables. As previously, there are negligible additional memory requirements for the coordinate system geometry other than the 2D derivatives of the topographic surface, T_2 and T_3.

The FSBC corresponding to the 3D unstretched topographic coordinate transform is given by

$$\frac{\partial v_1}{\partial \xi^1} = \zeta_T, \tag{55}$$

$$\frac{\partial v_2}{\partial \xi^1} = -\frac{\partial v_1}{\partial \xi^2} + 2 T_2 \zeta_T \tag{56}$$

$$\frac{\partial v_3}{\partial \xi^1} = -\frac{\partial v_1}{\partial \xi^3} + 2 T_3 \zeta_T \tag{57}$$

where

$$\begin{aligned} \zeta_T = & -E^{-1}_{(1-T_2^2-T_3^2),2} \left[\frac{\partial v_2}{\partial \xi^2} + \frac{\partial v_3}{\partial \xi^3} + T_2 \frac{\partial v_1}{\partial \xi^2} + \ldots \right. \\ & \left. T_3 \frac{\partial v_1}{\partial \xi^3} - \frac{\partial (T_2 v_1)}{\partial \xi_2} - \frac{\partial (T_3 v_1)}{\partial \xi_3} \right]. \end{aligned} \tag{58}$$

Again, the quantities in equations **??**-58 must be evaluated at the free surface (i.e., $\xi^1 = 0$).

Injection of a force source is given by

$$\left[\begin{array}{c} v_1 \\ v_2 \\ v_3 \end{array} \right] \Bigg|_{\boldsymbol{\xi}_0} = \left[\begin{array}{c} v_1 \\ v_2 + T_2 v_1 \\ v_3 + T_3 v_1 \end{array} \right] \Bigg|_{\boldsymbol{x}_0}, \tag{59}$$

while extraction of the particle velocity components from the computational grid is given by

$$\left[\begin{array}{c} v_1 \\ v_2 \\ v_3 \end{array} \right] \Bigg|_{\boldsymbol{x}_0} = \left[\begin{array}{c} v_1 \\ v_2 - T_2 v_1 \\ v_3 - T_3 v_1 \end{array} \right] \Bigg|_{\boldsymbol{\xi}_0}. \tag{60}$$

This completes the set of equations required to model 3D elastodynamics on a 3D unstretched topographic coordinate system.

4.2 Example 2: Linearly Stretched Topography

A second example is a computational mesh formed by a 3D linearly stretched topography mapping. This mapping can be applied by using a linear Bézier interpolation function (Shragge, 2014), which results in the following coordinate transformation:

$$F\left(\xi^1, \xi^2, \xi^3\right) = \xi^1 \left(1 - \frac{T(\xi^2, \xi^3)}{\alpha} \right) + T(\xi^2, \xi^3), \tag{61}$$

where $\xi^1 \in [0, \alpha]$; $T = T(\xi^2 = x^2, \xi^3 = x^3)$ is the topography at the free surface ($\xi^1 = 0$); and α is the maximum depth of the flat base of the coordinate system ($\xi_1 = x_1 = \alpha$). Figure 2 presents an depth section extracted from a 3D linearly stretched topographic coordinate mesh that uses the same topography as Figure 1, but slowly "heals" until reaching a flat base at a depth of $\xi_1 = \alpha = 8$ km.

Given the mapping in equation 61, it is straightforward to derive the derivative expressions of the F field:

$$\left[\begin{array}{c} F_1 \\ F_{1,1} \\ F_2 \\ F_3 \end{array} \right] = \left[\begin{array}{c} 1 - \frac{T}{\alpha} \\ 0 \\ T_2 \left(1 - \frac{\xi^1}{\alpha} \right) \\ T_3 \left(1 - \frac{\xi^1}{\alpha} \right) \end{array} \right]. \tag{62}$$

Solutions to the elastodynamics system for a linearly stretched topographic mesh can be found by replacing these fields in equations **??**-**??**. Applying the FSBC requires inserting these quantities into equations 31-36 and evaluating them at $\xi^1 = 0$ (i.e., $F_2|_{\xi^1=0} = T_2$ and $F_3|_{\xi^1=0} = T_3$). Similarly, performing wavefield injection or extraction requires introducing these quantities into equations 40 or 60 and evaluating the expressions at the relevant value of ξ^1. Unlike Example 1 above, the introduction of linear stretching leads to depth-dependent injection or extraction weighting factors.

4.3 Example 3: Internal Boundary

The final example of a computational mesh is one formed by a 3D internal boundary (IB) coordinate system that smoothly interpolates between upper and lower bounding surfaces and an internal boundary exhibiting topographic variations (e.g., a water bottom). A smooth interpolation between these three surface can

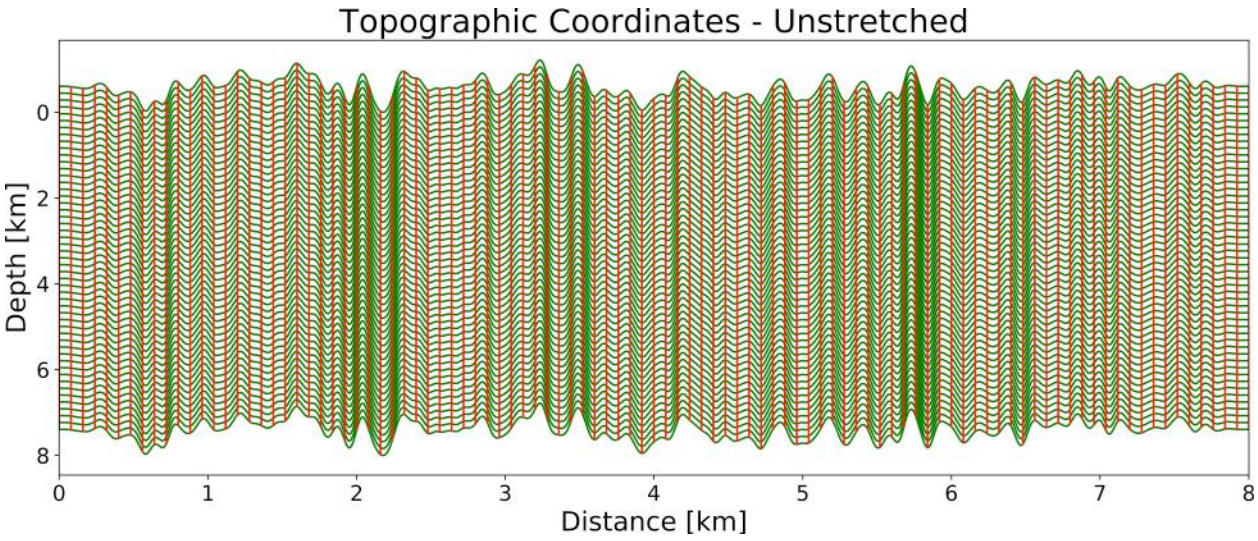

Figure 1. Depth section taken through a 3D unstretched topographic coordinate system. Note that the mesh is entirely defined by the topographic profile, T.

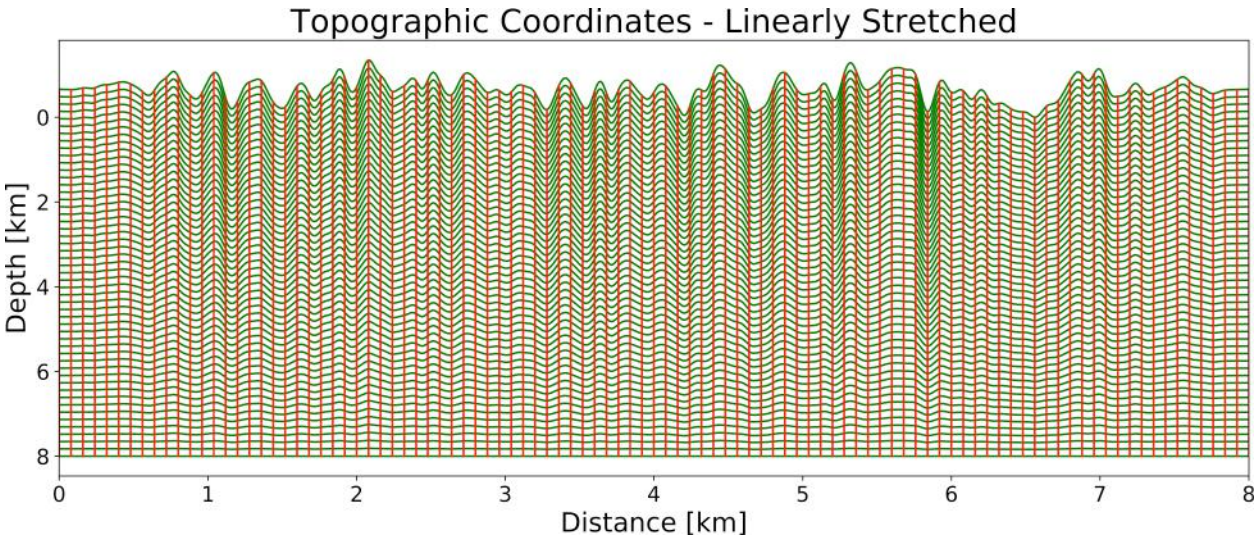

Figure 2. Depth section of a linearly stretched topographic coordinate mesh defined by the topographic profile, T, and the depth to the base of coordinate system, $\xi_1 = \alpha = 8$ km.

be developed using a quadratic Bézier interpolation formula:

$$F\left(\xi^1,\xi^2,\xi^3\right) = \frac{\xi^1}{\alpha\zeta(\zeta-1)}\left[W(\xi^2,\xi^3)(\xi^1-1)+\alpha\zeta(\zeta-\xi^1)\right], \tag{63}$$

where $W = W(\xi^2 = x^2, \xi^3 = x^3)$ is again the map of the topography of the internal boundary, ζ is the location of internal boundary surface within the coordinate mesh (i.e., $\zeta \in [0,1]$), and α is again the maximum depth of the flat base of the coordinate system. Figure 3 illustrates the 3D internal boundary coordinate mapping using a random surface, W, located halfway ($\zeta = 1/2$) through the mesh. Here, both the free-surface ($\xi_1 = 0$ m) and the base ($\alpha = 8$) km of the mesh are flat surfaces.

Again, with this mapping there will be lateral variation in the vertical sampling of the grid axis. Given the mapping in equation 63, the derivative expressions of the F field are given by:

$$\begin{bmatrix} F_1 \\ F_{1,1} \\ F_2 \\ F_3 \end{bmatrix} = \frac{1}{\alpha\zeta(\zeta-1)} \begin{bmatrix} W(2\xi^1-1)+\alpha\zeta(\zeta-2\xi^1) \\ 2(W-\alpha\zeta) \\ \xi^1(\xi^1-1)W_2 \\ \xi^1(\xi^1-1)W_3 \end{bmatrix}. \tag{64}$$

Solutions of the elastodynamics in a 3D internal boundary system can be found by introducing the fields in equation 64 into equations **??**-**??**. Similarly, evaluating the FSBC and performing injection or extraction are completed by inserting these quantities into equations 31-36 and equations 40 or 60, respectively. Note that unlike the previous two examples, for the 3D IB coordinate system $F_{1,1} \neq 0$ and we must now deal with a FSBC that has a dependence on both v_1 and $\frac{\partial v_1}{\partial \xi^1}$:

$$\frac{\partial v_1}{\partial \xi^1} = v_1 \frac{F_{1,1}}{F_1} - \frac{F_1^2}{E_{1,2}} \left(\frac{\partial v_2}{\partial \xi^2} + \frac{\partial v_3}{\partial \xi^3} \right), \quad (65)$$

$$\frac{\partial v_2}{\partial \xi^1} = -3 \frac{\partial v_1}{\partial \xi^2} + \frac{2}{F_1} \frac{\partial (F_1 v_1)}{\partial \xi_2}, \quad (66)$$

$$\frac{\partial v_3}{\partial \xi^1} = -3 \frac{\partial v_1}{\partial \xi^3} + \frac{2}{F_1} \frac{\partial (F_1 v_1)}{\partial \xi_3}, \quad (67)$$

where $F_1|_{\xi^1=0} = \frac{\alpha\zeta^2 - W}{\alpha\zeta(\zeta-1)}$ and $F_{1,1}|_{\xi^1=0} = \frac{2(W-\alpha\zeta)}{\alpha\zeta(\zeta-1)}$. Even though the free surface is flat, the laterally varying internal boundary mesh requires an altered FSBC to account for the non-constant F_1 and $F_{1,1}$ fields. The implication of this will be discussed in the section below. Finally, Cartesian equations of elastodynamics can be recovered by setting $\zeta = 1/2$ and $W = \alpha\zeta$.

5 DISCUSSION

The theory presented in the above sections has given rise to a number of observations that are worth additional discussion: memory and computational complexity; applying the FSBC; including additional control surfaces into vertically stretched meshes through higher-order Bézier interpolation functions; and the applicability of the above equations of 3D elastodynamics to other classes of numerical PDE solvers.

5.1 Memory and Computational Complexity

The tensorial equations of elastodynamics developed in the previous section have an advantage over other tensorial formulations in regards to memory complexity. The overall memory requirements relative to a Cartesian implementation are negligible since the memory requirements scale according to N^2 (assuming a cube with N points per side), while that of the stress and particle velocity memory variables scale by N^3. This is particularly advantageous in 3D FSG approaches involving four separate grids on different grid staggerings as it reduces the overall memory requirements and the degree of domain decomposition applied for large 3D meshes.

The use of equation 13 to remove the dependence on σ_k^i and v_j terms in equations 11 and 12 (and to help symmetrize the resulting system of equations), though, introduces additional stencil-based partial derivative calculations. While the values of F introduced in Examples 1-3 do eliminate some of the partial derivative calculations, there are still just under $2\times$ the number required for Cartesian implementations. However, the approach used in equation 13 assists with the overall short- and long-term numerical stability since each full time-step update involves only computing (weighted) second derivatives that are demonstrably more stability relative to systems involving first derivatives of the memory variables.

5.2 Applying the FSBC

The tensorial FSBC described above takes into account the spatially varying effects of a generalized mesh. The first term in the RHS of equation 31 potentially causes numerical issues since it explicitly depends on the vertical component of particle velocity, v_1, on the boundary. In Examples 1 and 2, the term $F_{1,1}$ is identically zero, which effectively forestalls this problem. However, due to the non-zero value of $F_{1,1}$ in Example 3, this potentially can pose numerical challenges.

The MFD+FSG solution advocated in the companion paper naturally handles these situations because a MFD scheme requires additional points on the boundary for all stress and particle velocity components on two of four subgrids. (This is required to satisfy the mimetic flux-preserving boundary conditions.) Accordingly, a 3D MFD+FSG scheme naturally handles the numerical challenges associated with implementing equation 31. However, the general applicability of the above analytic FSBC to other numerical schemes remains an open question.

5.3 Application to Other Vertically Deformed Meshes

The memory-efficient approach advocated above is based on the use of Bézier interpolation functions. However, there are (at least) two other approaches that can be used to develop more intricate computational meshes. First, one can apply higher-order Bézier interpolation schemes (i.e., greater than the $N = 2$ presented herein) that link together additional non-intersecting control surfaces into a single analytic coordinate system. Generally speaking, it is possible to link M surfaces together with a M^{th}-order Bézier interpolation functions; however, the complexity of this approach increases with the number of surfaces employed. A second approach would be to use a fully numerical F function that is output of some computational meshing algorithm. Following this approach would introduce an additional memory overhead of $2N^3$, and would represent a modest increase in computational complexity.

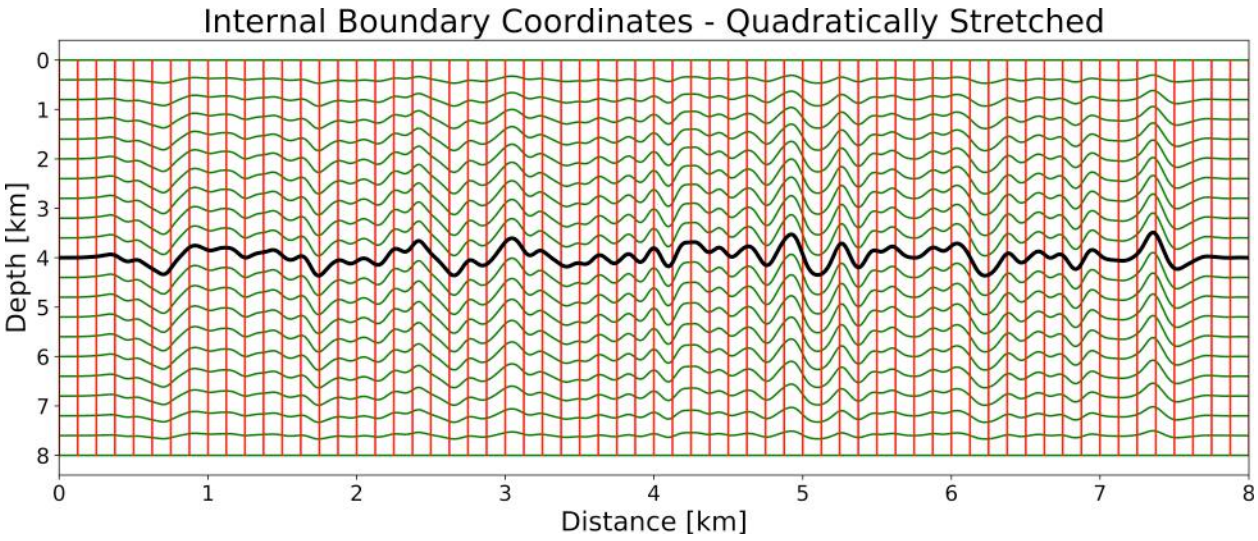

Figure 3. Cross-section of an Internal Boundary Coordinate system defined by a flat upper free surface ($\xi^3 = 0$ km), a flat lower surface (here $\alpha = 8.0$ km), and an irregular internal boundary later, $W = W(\xi_2, \xi_3)$ (illustrated with the thicker black line) here situated half-way through the internal boundary mesh (i.e., $\zeta = \frac{1}{2}$).

5.4 Application to other PDE solvers

Finally, while the companion paper follows a MFD-based numerical approach to solution, it is important to recognize that the above equations of 3D elastodynamics are generally applicable to other classes of numerical solvers. In particular, there are a number of available (e.g., finite-element) solvers that require specifying only the PDE and desired computational mesh. In this case one could feed the more complex 3D isotropic elastodynamics PDE and FSBC developed above - along with a regular cubic computational mesh ($\boldsymbol{\xi}$) - to simulate a 3D elastodynamics solution. One could then perform a high-order (e.g., sinc-based) interpolation from regular $\boldsymbol{\xi}$-computational mesh to recover the desired solution on the irregular physical ($\boldsymbol{x}$) coordinate system.

6 CONCLUSIONS

By deriving analytic equations of 3D elastodynamics for all permissible vertically deformed coordinate meshes, it is possible to specify a strategy for directly incorporating free-surface topography and internal boundaries that leads to straightforward implementations of the free-surface boundary condition. While this tensorial approach naturally fits with a MFD+FSG computational strategy, the equations are more generally applicable to other classes of numerical solution. Finally, validation of the derived equations and of the advocated MFD+FSG computational approach is left to companion paper, which provides a comparison with analytic expressions as well as a number of representative numerical examples.

7 ACKNOWLEDGMENTS

I acknowledge the support of Woodside Pty Ltd. and the Center for Wave Phenomena consortium sponsors. Analytic results were verified using the Mathematica software package.

APPENDIX A - METRIC TENSOR, COORDINATE TRANSFORMATIONS AND THE COVARIANT DERIVATIVE

The underlying geometry of many partial differential equations (PDEs) of mathematical physics, and their corresponding optimal solution domains, does not commonly lend itself to a straightforward numerical implementation in a Cartesian framework. In these situations, one of the most important strategies is to consider posing the underlying physical equations in a generalized coordinate system better suited to the characteristics of the particular geometry. While there are a number of coordinate representations that are particularly useful for solving problems with a high degree of symmetry (e.g., cylindrical or spherical coordinates), in most cases the topology of the solution domain requires a more general framework. The aim of this Appendix is to provide a brief overview of the tensorial approach of handling non-Cartesian meshes.

Without specifying an explicit coordinate system, one can define a generalized 3D coordinate system using a mapping relationship between the generalized coordinate variables, $\boldsymbol{\xi} = \left[\xi^1, \xi^2, \xi^3\right]$, and the underlying 3D Cartesian field, $\boldsymbol{x} = \left[x^1, x^2, x^3\right]$. The generalized map-

ping relationship, assumed to be invertible and one-to-one, is specified by a set of unique forward and inverse mapping equations

$$\xi^i = \xi^i(\boldsymbol{x}) \quad \text{and} \quad x^i = x^i(\boldsymbol{\xi}), \tag{A.1}$$

where a raised (lowered) index on the coordinate variables indicates a contravariant (covariant) coordinate basis. [For additional detail on the differences between these coordinate bases, the reader is referred to Synge and Schild (1978)]. The geometric connection between the two coordinate systems is the rank-two symmetric covariant metric tensor, $\mathbf{g}$, defined by

$$g_{ij} = \frac{\partial x^k}{\partial \xi^i}\frac{\partial x^k}{\partial \xi^j}, \tag{A.2}$$

where summation notation over repeated indices is assumed. The contravariant (inverse) metric tensor, g^{ij}, is computed by raising the indices of the metric tensor such that

$$g^{ij}g_{jk} = \delta^i_k = \delta^k_i, \tag{A.3}$$

where δ^i_k is Kroenker delta function. Note that when written in matrix notation this is equivalent to:

$$\left[g^{ij}\right] = \left[g_{ij}\right]^{-1}. \tag{A.4}$$

In developing the governing equations of elastodynamics in generalized coordinates one must first define how vector (i.e., a rank-one tensor) and higher-rank tensor quantities are affected by coordinate transformation. This can be achieved by applying a change of variables transformation. Of relevance to this particular study are the coordinate transformation of a covariant vector, v_i:

$$v_i|_{\boldsymbol{\xi}} = \frac{\partial x^j}{\partial \xi^i}\; v_j|_{\boldsymbol{x}} \tag{A.5}$$

where the domains in which quantities are being evaluated are explicitly indicated.

The second main transformation of interest is of a rank-two mixed (1,1) tensor, σ^i_j, given by

$$\sigma^i_j\Big|_{\boldsymbol{\xi}} = g^{ip}\frac{\partial x^k}{\partial \xi^p}\frac{\partial x^l}{\partial \xi^j}\;\sigma^k_l\Big|_{\boldsymbol{x}}, \tag{A.6}$$

where I introduce the inverse metric tensor to account for the one lowered index.

Applying differential operators on tensor fields requires developing expressions that account for the spatially varying coordinate geometry. Of relevance to this investigation is the covariant derivative ∇_j of a covariant vector field v_i. This operator can be expressed through "semi-colon" notation (i.e., $\nabla_j v_i \equiv v_{i;j}$), which is related to more familiar partial derivative expression through

$$v_{i;j} = \frac{\partial v_i}{\partial \xi^j} - \Gamma^k_{ij}v_k. \tag{A.7}$$

The Christoffel symbol of the second kind, Γ^k_{ij}, is related to spatial derivatives of the metric tensor components via

$$\Gamma^k_{ij} = \frac{1}{2}g^{km}\left(\frac{\partial g_{mi}}{\partial \xi^j} + \frac{\partial g_{mj}}{\partial \xi^i} - \frac{\partial g_{ij}}{\partial \xi^m}\right). \tag{A.8}$$

Note that Christoffel symbols are symmetric about the lower indices (i.e., $\Gamma^k_{ij} = \Gamma^k_{ji}$), and are not themselves tensors since they are not invariant under coordinate transformation. The covariant derivative of a mixed (1,1) stress tensor, $\nabla_c\sigma^a_b = \sigma^a_{b;c}$, is given by

$$\sigma^a_{b;c} = \frac{\partial \sigma^a_b}{\partial \xi^c} + \Gamma^a_{cd}\sigma^d_b - \Gamma^d_{cb}\sigma^a_d, \tag{A.9}$$

which is required for evaluating the conservation of linear momentum equation in equation 2 above.

REFERENCES

Appelö, D., and N. A. Petersson, 2009, A stable finite difference method for the elastic wave equation on complex geometries with free surfaces: Communications in Computational Physics, **5**, 84–107.

Brillouin, L., 1964, Tensors in mechanics and elasticity: Academic Press, New York, NY.

Carcione, J., 1994, The wave equation in generalized coordinates: Geophysics, **59**, 1911–1919.

Castillo, J., and G. Miranda, 2013, Mimetic Discretization Methods: CRC Press.

de la Puente, J., M. Ferrer, M. Hanzich, J. Castillo, and J. Cela, 2014, Mimetic seismic wave modelling including topography on deformed staggered grids: Geophysics, **79**, no. 3, T125–T141.

Faccioli, E., F. Maggio, R. Paolucci, and A. Quarteroni, 1997, 2d and 3d elasticwave propagation by a pseudo-spectral domain decomposition method: Journal of Seismology, **1**, no. 3, 237251.

Feng, K.-A., C.-H. Teng, and M.-H. Chen, 2007, A pseudospectral penalty scheme for 2d isotropic elastic wave computations: Journal of Scientific Computing, **33**, no. 3, 313–348.

Guo, H., 2014, Modern mathematics and applications in computer graphics and vision: World Scientific Publishing Company.

Hestholm, S., 1999, Three-dimensional finite difference viscoelastic wave modelling including surface topography: Geophysical Journal International, **139**, 852–878.

Hestholm, S., M. Moran, S. Ketcham, T. Anderson, M. Dillen, and G. McMechan, 2006, Effects of free-surface topography on moving seismic-source modeling: Geophysics, **71**, no. 6, T159–T166.

Hestholm, S., and B. Ruud, 2002, 3d free-boundary conditions for coordinate-transform finite-difference seismic modelling: Geophysical Prospecting, **50**, 463–474.

Käser, M., and M. Dumbser, 2006, An arbitrary high-order discontinuous Galerkin method for elastic waves

on unstructured meshes - I. The two-dimensional isotropic case with external source terms: Geophysical Journal International, **166**, no. 2, 855–877.

Komatitsch, D., F. Coutel, and P. Mora, 1996, Tensorial formulation of the wave equation for modelling curved interfaces: Geophysical Journal International, **127**, 156–168.

Komatitsch, D., and J.-P. Vilotte, 1998, The spectral element method; an efficient tool to simulate the seismic response of 2D and 3D geological structures: Bulletin of the Seismological Society of America, **88**, no. 2, 368–392.

Lebedev, V., 1964, Difference analogues of orthogonal decompositions, basic differential operators and some boundary value problems: USSR Computational Mathematics and Mathematical Physics, **4**, 449–465.

Lisitsa, V., and D. Vishnevskiy, 2010, Lebedev scheme for the numerical simulation of wave propagation in 3D anisotropic elasticity: Geophysical Prospecting, **58**, 619–635.

Lombard, B., J. Piraux, C. Gelis, and J. Virieux, 2008, Free and smooth boundaries in 2-D finite-difference schemes for transient elastic waves: Geophysical Journal International, **172**, no. 1, 252–261.

McConnell, A., 1957, Applications of tensor analysis: Dover Publications, New York, NY.

Shragge, J., 2014, Solving the generalized 3d acoustic wave equation: Geophysics, **82**, no. 6, T363–T378.

Shragge, J., and B. Tapley, 2017, Solving the Tensorial 3D Acoustic Wave Equation: A Mimetic Finite-Difference Time-Domain Approach: Geophysics, **82**, no. 4, T183–T196.

Synge, J., and A. Schild, 1978, Tensor Calculus: Dover Publications, Inc., New York.

Tromp, J., D. Komatitsch, and Q. Liu, 2008, Spectral-element and adjoint methods in seismology: Communications in Computational Physics, **3**, no. 1, 1–32.

Zhang, W., and X. Chen, 2006, Traction image method for irregular free surface boundaries in finite difference seismic wave simulation: Geophysical Journal International, **167**, no. 1, 337–353.